3COMPDYN 2017
6th ECCOMAS Thematic Conference on
Computational Methods in Structural Dynamics and Earthquake Engineering
M. Papadrakakis, M. Fragiadakis (eds.)
Rhodes Island, Greece, 15–17 June 2017

CONSIDERING STRUCTURAL MODELLING UNCERTAINTIES USING BAYESIAN CLOUD ANALYSIS

Andrea Miano[1], **Fatemeh Jalayer**[1], **Andrea Prota**[1],

[1)] Department of Structures for Engineering and Architecture, University of Naples "Federico II"
Via Claudio 21, 80125, Naples, Italy
{andrea.miano, fatemeh.jalayer, a.prota}@unina.it

Keywords: Performance based seismic assessment; existing structures, epistemic uncertainties; Monte Carlo simulation; Structural Collapse.

Abstract. *Quantifying the impact of modelling uncertainty on the seismic performance assessment is a crucial issue for existing buildings, considering the partial information available related to material properties, construction details and the uncertainty in the capacity models. The effect of structural modelling uncertainties on the seismic performance of existing buildings can be –under certain circumstances- comparable to that of uncertainty in ground motion representation. In this work, a modified version of Cloud analysis considering the (eventual) cases of global dynamic instability and adopting the critical demand to capacity ratio as the damage measure/decision variable, based on coupling the simple regression in the logarithmic space of structural response versus seismic intensity for a suite of registered records with logistic regression, has been implemented to consider the record-to-record variability, structural modelling uncertainties and the uncertainties in the parameters of the adopted fragility model. For each of the registered records within the suite of ground motion records, a different realization of the structural model has been generated through a standard Monte Carlo Simulation procedure. A Bayesian version of the Cloud method is employed, in which the uncertainty in the structural fragility model parameters is considered. This leads to a robust fragility estimate—reflecting both record-to-record variability and structural modeling uncertainties-- and a desired confidence interval defined around it –reflecting the uncertainty in the fragility model parameters. The longitudinal frame of an existing building in Van Nuys, CA, modeled in OpenSees considering the flexural-shear-axial interaction, has been employed in order to demonstrate this procedure. The critical demand to capacity ratio adopted as the damage measure/decision variable, corresponding to the component or mechanism that leads the structure closest to the onset of limit state (e.g., near collapse), is adopted as the structural response parameter. This structural response parameter can encompass both ductile and fragile failure mechanisms. Moreover, it can register a possible shift in the governing failure mechanism with increasing intensity. The selection of the suite of ground motion records has been based on a set of criteria that ensure the statistical significance of the linear regression in predicting the structural response as a function of the intensity measure.*

1 INTRODUCTION

Assessment of analytic structural fragility for existing buildings is one of the fundamental steps in the modern performance-based engineering [1]. One main feature distinguishing the assessment of existing buildings from that of the new ones is the large amount of uncertainty present in determining the structural modeling parameters. In particular, considering the partial information available related to material properties, construction details and also the uncertainty in the capacity models, the impact of modelling uncertainties on the seismic performance assessment is a crucial issue for existing buildings. Thus, for this type of buildings, explicit consideration of modelling uncertainty in the process of the assessment of structural performance can lead to more accurate results.

In order to assess the performance of the existing buildings, there are alternative non-linear dynamic analysis procedures available in the literature. These methods, such as, Incremental Dynamic Analysis (IDA, [2]), Multiple-Stripe Analysis (MSA, [3-5]) and Cloud Analysis [3,6-9], characterize the fragility, expressed as the conditional probability of exceeding a prescribed limit state given the seismic intensity and by employing recorded ground motions. Cloud Analysis is particularly efficient since it involves the non-linear analysis of the structure subjected to a set of un-scaled ground motion time-histories. The simplicity of its underlying formulation makes it a quick and efficient analysis procedure for fragility assessment [10]. However, Cloud Analysis is also notorious for being based on a few simplifying assumptions (fixed standard error of regression, mean response varying linearly as a function of IM in the logarithmic scale, and structural response given IM being modeled as a Lognormal distribution), and for being very much sensitive to the selected suite of records [8-9]. Cloud Analysis has been used, not only to model the record-to-record variability in ground motion, but also to propagate structural modelling uncertainties such as uncertainty in component capacity [8,11] and the uncertainties in mechanical material properties and construction details [8,12]. One approximate way to consider the epistemic uncertainties in the fragility assessment is to consider the uncertainty in the evaluation of the median of the fragility curve (e.g., [10-11,13-17]). Such modelling of epistemic uncertainties, assuming that the median is unbiased and normally distributed, leads to an overall increase in the fragility dispersion and leaves the fragility median invariant. In other words, such procedure does not manage to capture the bias in median limit state probability due the effect of epistemic uncertainties. Simulation-based methods are arguably the most efficient and straightforward means for taking into account the epistemic uncertainties (see e.g., [18-19]). However, they fall short of modelling record-to-record variability when recorded ground motions are implemented (due to a lack of reference probability distributions for recorded ground motions). In the recent years, several alternative methods have been proposed that combine reliability methods such as the first order second moment (FOSM and MVFOSM, see for example [20]) methods, response surface methods [21], simulation-based methods (e.g., Monte Carlo, Latin Hypercube Sampling) with non-linear dynamic procedures such as IDA based on recorded ground motions in order to take into account also sources of uncertainties other than record-to-records variability [22-25].

In this work, a modified version of Cloud Analysis considering the (eventual) cases of global dynamic instability, based on coupling the simple regression in the logarithmic space of structural response versus seismic intensity for a suite of registered records with logistic regression, has been implemented to consider both record-to-record variability and modelling uncertainties. This modified version of Cloud Analysis relies on adopting a critical demand to capacity ratio, which is equal to unity at the onset of limit state, as the damage measure/decision variable. This structural response parameter can encompass both ductile and

fragile failure mechanisms. Moreover, it can register a possible shift in the governing failure mechanism with increasing intensity. For each of the registered records within the suite of ground motion records, a different realization of the structural model has been generated through a standard Monte Carlo Simulation procedure. A Bayesian updating framework, which treats the structural response to the selected records as "data", is adopted to take into account the uncertainty in the fragility parameters. One advantage in using the Bayesian framework is that it leads to fragility estimation together with the definition of a prescribed confidence band. Consequently, the risk estimates can be provided as a range of values that map a certain probability content in terms of the confidence in the fragility estimate (e.g., plus/minus one or two standard deviations from the median that correspond to approximately 70% and 95% probability content, respectively, assuming Normality). There are no specific restrictions on the sample of "data" points other than being plausible independent "observations" (in reality they are calculated) of the structural response. Another advantage in using such framework is that it enables the formal introduction of prior information available about the fragility parameters (e.g., particularly useful for updating of existing fragility models).

The longitudinal frame of a seven-story existing building in Van Nuys, CA, which has been modeled in OpenSees considering the flexural-shear-axial interactions, has been employed to demonstrate this procedure. The selection of the suite of ground motion records has been performed based on a set of criteria that ensure the statistical significance of the linear regression in predicting the structural response as a function of the intensity measure.

2 METHODOLOGY

The methodology for the assessment of the robust structural fragility and its prescribed confidence interval based on Cloud Analysis and considering explicitly the cases of "collapse" has been documented in detail in [9] considering only record-to-record variability. This paper employs this method to consider also the structural modeling uncertainties. Below, a brief description of this method is reported.

2.1 The Intensity Measure and the Structural Performance Variable

The original framework for performance-based earthquake engineering (PBEE, [26]) propagates the various sources of uncertainty in the structural performance assessment through adopting a series of generic variables representing the seismic intensity (intensity measure, IM), the structural response (engineering demand parameter, EDP), the structural damage (damage measure, DM), and the structural performance (decision variable, DV). Herein, the critical demand to capacity ratio for a prescribed limit state [11] and denoted as DCR_{LS}, has been adopted as a proxy for the structural performance variable (DV). This DV is going to be convoluted directly with the intensity measure (IM) in order to estimate the seismic risk in the PBEE framework. DCR_{LS} is defined as the demand to capacity ratio for the component or mechanism that brings the system closer to the onset of limit state *LS*. The formulation is based on the cut-set concept [27], which is suitable for cases where various potential failure mechanisms (both ductile and fragile) can be defined a priori. DCR_{LS}, which is always equal to unity at the onset of limit state, is defined as:

$$DCR_{LS} = \max_{l}^{N_{mech}} \min_{j}^{N_l} \frac{D_{jl}}{C_{jl}(LS)} \tag{1}$$

where N_{mech} is the number of considered potential failure mechanisms; N_l is the number of components taking part in the lth mechanism; D_{jl} is the demand evaluated for the jth structural component of the lth mechanism; $C_{jl}(LS)$ is the limit state capacity for the jth component of the lth mechanism.

In this work, the critical demand to capacity ratio is going to be evaluated for the near collapse limit state [28]. The component demand to capacity ratios are expressed in terms of the maximum component chord rotation. This leads to a deformation-based DCR_{LS}. The maximum chord rotation demand D_{jl} for the j^{th} component of the l^{th} mechanism is obtained from the results of the nonlinear dynamic analysis. The component chord rotation capacity C_{jl} for the j^{th} component of the l^{th} corresponds to the ultimate capacity of the member. For the near collapse limit state it is defined as the point on the softening branch of the force-deformation curve of the component, where a 20% reduction in the maximum strength takes place (Eurocode 8, Part 3). In this study, the possible failure mechanisms associated with the near-collapse limit state correspond to ductile or brittle failures of the columns; i.e., $DCR_{LS}>1$ for a column is achieved when $D_{jl} > C_{jl}$ where D_{jl} and C_{jl} for each column are obtained by taking into account the flexural/axial behavior, the shear behavior and the fixed-end rotation due to bar slip.

When predicting non-linear response of structures for an ultimate limit state, it is common to encounter a few records leading to global "*Collapse*"; i.e., very high global displacement-based demands or non-convergence problems in the analyzing software. Obviously, $DCR_{LS}>1$ for the near-collapse limit state does not necessary imply the occurrence of global Collapse. Herein, the global *Collapse* of the structure is identified explicitly by verifying the following two criteria: (1) accounting for the loss of load bearing capacity when 50% +1 of the columns of a story reach the chord rotation corresponding to the complete loss of vertical-load carrying capacity of the component [29]; (2) accounting for for global dynamic instability when maximum inter-story drift exceeds 10%.

2.2 The "observed data" D

Let vector θ represent all the uncertain parameters considered in the problem (apart from the fragility model parameters and those related to the ground motion representation). For example, this vector may contain component capacity model parameters, construction detail parameters and parameters related to mechanical material properties. It is enough to note that any given realization θ_i of vector θ identifies in a unique manner the structural model. Ideally, a standard Monte Carlo simulation can be used for generating a set of i=1:N realizations of the vector θ.

In particular, for each of the registered records within the suite of ground motion records, a different realization of the structural model has been generated through a standard Monte Carlo Simulation procedure. This way, each realization of the vector θ (plausible structural model subjected) subjected to a registered record leads to the corresponding DCR value. The set of DCR values calculated this way are then used as "observed data" in order to update the probability distribution for the parameters of the prescribed fragility model (e.g., Lognormal).

2.3 A regression-based probabilistic model for predicting DCR_{LS} given IM (Cloud Analysis)

Herein, a regression-based probability model is employed to describe the DCR_{LS} for a given IM level. Let $DCR_{LS}=\{DCR_{LS,i},\ i=1:N\}$ be the set of critical demand to capacity ratio for limit state *LS*, calculated through non-linear time-history analyses performed for a suite of N recorded ground motions, and $S_a=\{S_{a,i},\ i=1:N\}$ be the set of corresponding spectral acceleration values (where $DCR_{LS,i}$ and $S_{a,i}$ are calculated for the ith ground motion record). The *Cloud data* or simply *data* hereafter refer to the set $\mathbf{D}=\{(S_{a,i}, DCR_{LS,i}),\ i=1:N\}$. The regression probabilistic model can be described as follows:

$$\mathbb{E}[\ln DCR_{LS} \mid S_a] = \ln \eta_{DCR_{LS}|S_a} = \ln a + b \ln S_a \,,\; \sigma_{\ln DCR_{LS}|S_a} = \sqrt{\sum_{i=1}^{N} \left(\ln DCR_{LS,i} - \ln \eta_{DCR_{LS}|S_{a,i}} \right)^2 \Big/ (N-2)} \qquad (2)$$

where $\mathbf{E}[\ln DCR_{LS}|S_a]$ is the expected value for the natural logarithm of DCR_{LS} given S_a; $\eta_{DCRLS|Sa}$ is the median for DCR_{LS} given S_a; $\sigma_{\ln DCRLS|Sa}$ is the logarithmic standard deviation for DCR_{LS} given S_a. This non-linear dynamic analysis procedure, also known as the *Cloud Analysis* (e.g.,[]), graphically invokes the idea of the scatter plot of data pairs of structural performance variable and the intensity measure for a given ground motion record. The Cloud Analysis is particularly useful when one deals with un-scaled ground motion records. The structural fragility obtained based on the Cloud Analysis can be expressed as the probability that DCR_{LS} exceeds unity given S_a:

$$P(DCR_{LS} > 1 | S_a, \boldsymbol{\chi}] = P(\ln DCR_{LS} > 0 | S_a, \boldsymbol{\chi}) = 1 - \Phi\left(\frac{-\ln \eta_{DCR_{LS}|S_a}}{\sigma_{\ln DCR_{LS}|S_a}} \right) = \Phi\left(\frac{\ln \eta_{DCR_{LS}|S_a}}{\beta_{DCR_{LS}|S_a}} \right) \qquad (3)$$

where $\Phi(\cdot)$ is the standardized Gaussian Cumulative Distribution Function (CDF), $\boldsymbol{\chi}$=[ln$a$, b, $\beta_{DCRLS|Sa}$] denotes the model parameters and $\beta_{DCRLS|Sa} \triangleq \sigma_{\ln DCRLS|Sa}$. Note that Eqn 3 is a three-parameter fragility model which can be determined as a function of known vector $\boldsymbol{\chi}$.

2.4 Cloud Analysis considering collapse and/or global dynamic instability

This section illustrates that, with some modifications, the Cloud Analysis can still be carried out in the cases in which some records take the structure to verge upon "Collapse". Let the Cloud data be partitioned into two parts: (a) *NoC* data which correspond to that portion of the suite of records for which the structure does not experience "Collapse", (b) *C* corresponding to the "Collapse"-inducing records. The structural fragility for a prescribed limit state *LS*, expressed in Eqn 3, can be expanded with respect to *NoC* and *C* sets using Total Probability Theorem (see [4,30]):

$$P\left(DCR_{LS} > 1 | S_a\right) = P\left(DCR_{LS} > 1 | S_a, NoC\right) \cdot \left(1 - P(C | S_a)\right) + P\left(DCR_{LS} > 1 | S_a, C\right) \cdot P\left(C | S_a\right) \qquad (4)$$

where $P(DCR_{LS}>1|S_a,NoC)$ is the conditional probability that DCR_{LS} is greater than unity given that "Collapse" has not taken place (*NoC*) and can be described by a Lognormal distribution (a widely used assumption that has been usually verified for maximum inter-story drift response given intensity in cases where the regression residuals represent unimodal behavior, e.g., [4,6]):

$$P\left(DCR_{LS} > 1 | S_a, NoC\right) = \Phi\left(\frac{\ln \eta_{DCR_{LS}|S_a,NoC}}{\beta_{DCR_{LS}|S_a,NoC}} \right) \qquad (5)$$

where $\eta_{DCRLS|Sa,NoC}$ and $\beta_{DCRLS|Sa,NoC}$ are conditional median and logarithmic standard deviation (dispersion) of DCR_{LS} for *NoC* portion of the data. $P(DCR_{LS}>1|S_a,NoC)$ is calculated in exactly the same manner as the standard Cloud Analysis discussed in Section 2.2 (see Eqn 3). The term $P(DCR_{LS}>1|S_a,C)$ is the conditional probability that DCR_{LS} is greater than unity given "Collapse". This term is equal to unity, i.e., in the cases of "Collapse", the limit state *LS* (herein, Near-Collapse) is certainly exceeded. Finally, $P(C|S_a)$ in Eqn 4 is probability of collapse, which can be predicted by a logistic regression model (a.k.a., logit) as a function of S_a (see also [31], and expressed as follows:

$$P\left(C | S_a\right) = \frac{1}{1 + e^{-\left(\alpha_0 + \alpha_1 \cdot \ln(S_a)\right)}} \qquad (6)$$

where α_0 and α_1 are the parameters of the logistic regression. It is to note that the logistic regression model belongs to the family of generalized regression models and is particularly useful for cases in which the regression dependent variable is binary (i.e., can have only two values 1 and 0, *yes* or *no*, which is the case of *C* and *NoC* herein). Note that the logistic re-

gression model described above is applied to all records; they are going to be distinguished by 1 or 0 depending on whether they lead to collapse or not. Finally, the analytic fragility model in the case where the data includes "collapse-cases" can be obtained by substituting the terms $P(DCR_{LS}>1|S_a,NoC)$ and $P(C|S_a)$ from Eqns 5 and 6 into Eqn 4:

$$P\left(DCR_{LS}>1\middle|S_a,\boldsymbol{\chi}\right)=\Phi\left(\frac{\ln\eta_{DCR_{LS}|S_a,NoC}}{\beta_{DCR_{LS}|S_a,NoC}}\right)\cdot\frac{e^{-\left(\alpha_0+\alpha_1\ln(S_a)\right)}}{1+e^{-\left(\alpha_0+\alpha_1\ln(S_a)\right)}}+\frac{1}{1+e^{-\left(\alpha_0+\alpha_1\ln(S_a)\right)}} \tag{7}$$

Eqn 7 illustrates a five-parameter fragility model whose model parameters can be denoted as $\boldsymbol{\chi}=[\ln a,\ b,\ \beta_{DCRLS|NoC,Sa},\ \alpha_0,\ \alpha_1]$. Given $\boldsymbol{\chi}$, the fragility can be perfectly determined (for simplicity, $\beta_{DCRLS|NoC,Sa}$ is replaced with β hereafter). The CDF of $DCR_{LS}|S_a$ for a given demand to capacity ratio dcr can be derived as follows based on Total Probability Theorem:

$$\begin{aligned}P\left(DCR_{LS}\le dcr\middle|S_a\right)&=P\left(DCR_{LS}\le dcr\middle|S_a,NoC\right)P\left(NoC\middle|S_a\right)+P\left(DCR_{LS}\le dcr\middle|S_a,C\right)P\left(C\middle|S_a\right)\\&=\Phi\left(\frac{\ln dcr-\ln\eta_{DCR_{LS}|S_a,NoC}}{\beta_{DCR_{LS}|S_a,NoC}}\right)P\left(NoC\middle|S_a\right)\end{aligned} \tag{8}$$

where it has been assumed that $P(DCR_{LS}\le dcr\ |C,S_a)=0$ assuming that DCR_{LS} is going to be un-boundedly large for the collapse cases. Eqn 8 can be used in order to calculate the value $dcr=DCR^p$ corresponding to the percentile p by setting the left side of the Eqn 8 equal to p and solving it for DCR^p:

$$DCR^p=\eta_{DCR_{LS}|S_a,NoC}\cdot\exp\left(\beta_{DCR_{LS}|S_a,NoC}\cdot\Phi^{-1}\left[p/P(NoC\mid S_a)\right]\right) \tag{9}$$

where Φ^{-1} is the inverse function of standardized normal distribution. For example, the above equation can be used the 16th, 50th and 84th percentile curves of DCR versus spectral acceleration.

2.5 Robust Fragility assessment (using simulation)

Inspired from the concept of updated robust reliability [18,32], the *Robust Fragility* is defined as the expected value for a prescribed fragility model taking into account the joint probability distribution for the (fragility) model parameters $\boldsymbol{\chi}$ [8,12,31]. The Robust Fragility can be written as:

$$P\left(DCR_{LS}>1\middle|S_a,\mathbf{D}\right)=\int_{\Omega_{\boldsymbol{\chi}}}P\left(DCR_{LS}>1\middle|S_a,\boldsymbol{\chi}\right)f(\boldsymbol{\chi}|\mathbf{D})\,\mathrm{d}\boldsymbol{\chi}=\mathbb{E}_{\boldsymbol{\chi}}\left[P\left(DCR_{LS}>1\middle|S_a,\mathbf{D},\boldsymbol{\chi}\right)\right] \tag{10}$$

where $\boldsymbol{\chi}$ is the vector of fragility model parameters and $\boldsymbol{\Omega}_{\boldsymbol{\chi}}$ is its domain; $f(\boldsymbol{\chi}|\mathbf{D})$ is the joint probability distribution for fragility model parameters given the vector of Cloud data $\mathbf{D}$ (see Section 2.2). The term $P(DCR_{LS}>1|S_a,\boldsymbol{\chi})$ is the fragility model given that the vector $\boldsymbol{\chi}$ is known (see Eqn 3 or Eqn 7). Note that it has been assumed that the vector $\boldsymbol{\chi}$ is sufficient to describe the data $\mathbf{D}$ (that is why $\mathbf{D}$ has been dropped from the right-hand side of the conditioning sign |). $\mathbf{E}_{\boldsymbol{\chi}}(\cdot)$ is the expected value over the vector of fragility parameters $\boldsymbol{\chi}$. The variance σ^2 in fragility estimation can be calculated as:

$$\sigma^2_{\boldsymbol{\chi}}\left[P\left(DCR_{LS}>1\middle|S_a,\mathbf{D},\boldsymbol{\chi}\right)\right]=\int_{\Omega_{\boldsymbol{\chi}}}P\left(DCR_{LS}>1\middle|S_a,\boldsymbol{\chi}\right)^2f(\boldsymbol{\chi}|\mathbf{D})\,\mathrm{d}\boldsymbol{\chi}-\mathbb{E}^2_{\boldsymbol{\chi}}\left[P\left(DCR_{LS}>1\middle|S_a,\mathbf{D},\boldsymbol{\chi}\right)\right] \tag{11}$$

Note that calculating the variance over the vector of fragility parameters $\boldsymbol{\chi}$ from Eqn 11, i.e. $\sigma^2_{\boldsymbol{\chi}}(\cdot)$, provides the possibility of estimating a confidence interval of for the fragility considering the uncertainty in the estimation of the fragility model parameters. The integrals in Eqn 10 and Eqn 11 in general do not have analytic solutions and should be solved numerically. Simulation schemes provide very efficient means for numerical resolution of an integral. Herein, a very efficient simulation scheme known as Markov Chain Monte Carlo (MCMC) Simulation

is employed in order to sample from $f(\boldsymbol{\chi}|\mathbf{D})$ and solve the integral in Eqs. 10 and 11, as proposed in [9].

2.6 Implementing the concept of Robust Fragility in order to take into account the structural modeling uncertainties

This paper implements the concept of Robust Fragility in order to efficiently propagate the sources of uncertainty related to both record-to-record variability and structural modelling, based on the results of a Cloud Analysis. In particular, the Cloud procedure is embedded in a Bayesian updating framework that updates the distribution of the fragility model parameters (based on the Cloud Analysis results) in order to lead to robust fragility estimates and the confidence bands. The flowchart in Figure 1 describes this procedure in a step-by-step manner:

Step 1: Perform the record selection. In this step, the record selection for Cloud Analysis should be performed, based on very few main rules. That is, the records should be selected in a way that they cover a vast range of spectral acceleration values and the records should be selected so that a significant proportion of records have DCR_{LS} greater than unity.

Step 2: Characterize the uncertainties vector θ and the associated joint PDF, where θ represents all the uncertain parameters in the problem related to structural modeling. For example, as previously explained, this vector may contain component capacity modelling parameters, construction detailing parameters, parameters related to mechanical material properties and parameters related to the ground motion representation. It is enough to note that any given realization θ_i of vector θ identifies in a unique manner the structural model.

Step 3: Generate n samples (with MC simulation, LHS, …, etc.) of the vector θ, where n is the number of the records. Note that for each of the registered records within the suite of ground motion records, a different realization of the structural model is generated through for example a standard Monte Carlo Simulation procedure or a Latin Hypercube Sampling.

Step 4: Subject each structural model configuration to one of the records within the set. In this way, each realization of the vector θ (plausible structural model subjected to a registered record) leads to a corresponding critical DCR_{LS} value.

Step 5: Form the set of the critical $DCR_{LS}=\{DCR_{LS,i},\ i=1:N_{records}\}$ and perform Cloud Analysis. As said in sections 2.3 and 2.4, Cloud Analysis is based on a regression-based probability model, that is employed to describe the DCR_{LS} for a given IM level. Let $DCR_{LS}=\{DCR_{LS,i},\ i=1:N\}$ be the set of critical demand to capacity ratio for limit state *LS*, calculated through non-linear time-history analyses performed for the set of N records, and $S_a=\{S_{a,i},\ i=1:N\}$ be the set of corresponding spectral acceleration values (where $DCR_{LS,i}$ and $S_{a,i}$ are calculated for the ith record). The *Cloud data* refer to the set $\mathbf{D}=\{(S_{a,i},\ DCR_{LS,i}),\ i=1:N\}$. If cases in which some records take the structure to verge upon "Collapse" are present, the Cloud data can be partitioned into two parts (e.g. No Collapse data and Collapse data). The structural fragility can be expanded with respect to No Collapse and Collapse sets using Total Probability Theorem as explained in Eqn. 4

Step 6: Obtain the Robust Fragility and the desired confidence bands. This entails Updating the joint distribution (χ|D) for the fragility model parameters χ, based on the cloud data D (see sect. 2.5) and simulating vector $\boldsymbol{\chi}_i$ based on its probability density function $f(\boldsymbol{\chi}|\mathbf{D})$. This leads to the solution of the integrals leading to the Robust Fragility and its standard deviation (Eqs. 10 and 11).

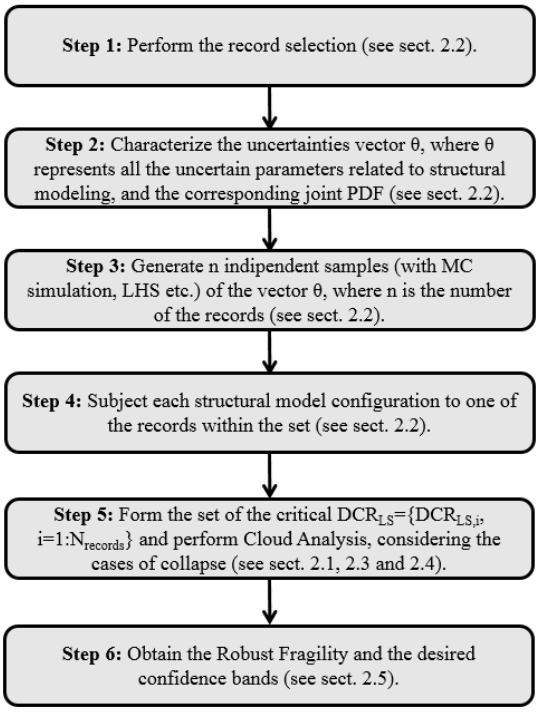

Figure 1 Step-by-step guide to implementing the Robust Fragility procedure for propagating both record-to-record variability and structural modelling uncertainties.

3 NUMERICAL APPLICATION

3.1 Case-study structure and model description

One of the longitudinal frames of the seven-story hotel building in Van Nuys, California, is modeled and analyzed in this study. The building is located in the San Fernando Valley of Los Angeles County (34.221° north latitude, 118.471° west longitude). The frame building was constructed in 1966 according to the 1964 Los Angeles City Building Code. The building was damaged in the M6.7 1994 Northridge earthquake. After the 1994 earthquake, the building was retrofitted with addition of new RC shear walls. Columns in the longitudinal frame are 356 mm wide and 508 mm deep, i.e., they are oriented to bend in their weak direction when resisting lateral forces in the plane of the longitudinal frame. Spandrel beams in the north frame are typically 406 mm wide and 762 mm deep in the second floor, 406 mm wide and 572 mm deep in the third through seventh floors, and 406 mm by 559 mm at the roof level. Column concrete has a compressive nominal strength f'_c of 34.5 MPa in the first story, 27.6 MPa in the second story, and 20.7 MPa in other floors. Beam and slab concrete strength f'_c is 27.6 MPa in the second floor and 20.7 MPa in other floors. Grade 60 (f_y=414 MPa) reinforcing steel is used in columns. The specified yield strength, f_y, is 276 MPa (Grade 40) for the steel used in beams and slabs. Figure 2 shows the longitudinal frame modeled in this research and some of the damaged columns in this frame after the 1994 Northridge earthquake.

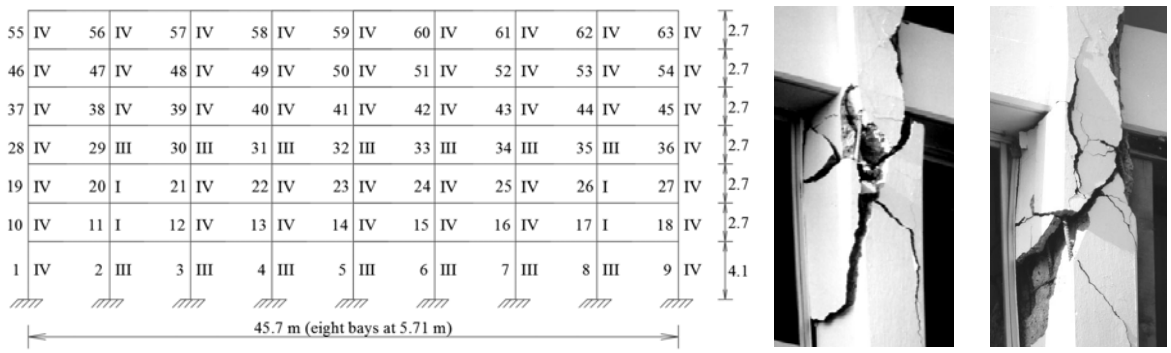

Figure 2 Holiday Inn hotel building longitudinal frame and some of the damaged columns in this frame after the 1994 Northridge earthquake.

3.1.1. Flexural model

Unidirectional axial behavior of concrete and steel materials are modeled to simulate the nonlinear response of beams and columns. Concrete material response is simulated using the Concrete01 material in OpenSees [33], which includes zero tensile strength and a parabolic compressive stress-strain behavior up to the point of maximum strength with a linear deterioration beyond peak strength. Because the transverse reinforcement ratio for beams and columns in the Van Nuys building is relatively low and detailing does not meet the modern seismic code requirements, concrete is modeled more close to the unconfined concrete model with peak strength achieved at a strain of 0.002 and minimum post-peak strength achieved at a compressive strain of 0.006. The corresponding strength at ultimate strain is $0.05f'_c$ for f'_c=34.5 MPa and f'_c=27.6 MPa, and $0.2f'_c$ for f'_c=20.7 MPa.

Longitudinal steel behavior is simulated using the Steel02 material in OpenSees. This model includes a bilinear stress-strain envelope with a curvilinear unload-reload response under cyclic loading. The previous research indicates that the observed yield strength of reinforcing steel exceeds the nominal strength [34,35]. Following the recommendation of [35], yield strength of 345 MPa (50 ksi) and 496 MPa (72 ksi) are used in this research for Grade 40 and Grade 60 steel, respectively. Both Grade 40 and Grade 60 reinforcement are assumed to have a post-yielding modulus equal to 1% of the elastic modulus, which is assumed to be 200 GPa. Additional parameters required to define the Steel02 material model are taken equal to those recommended in the OpenSees User's Manual. Uniaxial fibers within the gross cross section were assigned either concrete (Concrete 01) or steel (Steel 02). A typical column cross section included 30 layers of axial fibers, parallel to the depth of the section. Effective slab width was included in beam cross sections. Flexural response of beams and columns are simulated using fiber cross sections, representing the beam-column line elements Figure 3(a).

In OpenSees, flexural beam-column members are modeled as force-based in which an internal element solution determines member deformations that satisfy the system compatibility. In force-based column elements, distributed plasticity model is used to accurately determine yielding and plastic deformations at the integration points along the element length under increasing loads. Newton-Cotes integration [36] is selected as a suitable numerical integration solution for the force-based column element to accurately capture plastic deformations along the members. Newton-Cotes method distributes integration points uniformly along the length of the element. Herein, five integration points is used including one point at each end of the element, as shown in Figure 3(b). Force-deformation response of beam elements is computed based on the assumption that inelastic action occurs mainly at the member ends and that the middle of the member remains typically elastic (however, this is not necessary). Therefore, plastic hinge integration methods are used to confine nonlinear deformations in end regions of

beam elements, while the remainder of the element is assumed to stay linear elastic. It is assumed that the length of plastic region is equal to the depth of the cross-section. The modified Gauss Radau hinge integration method [36] is used for numerical integration of the force-based beam elements where the integration within each hinge region is implemented at four points; two integration points in the element ends, and two at 8/3 of the hinge length, $L_o=h$, as illustrated in Figure 3(c).

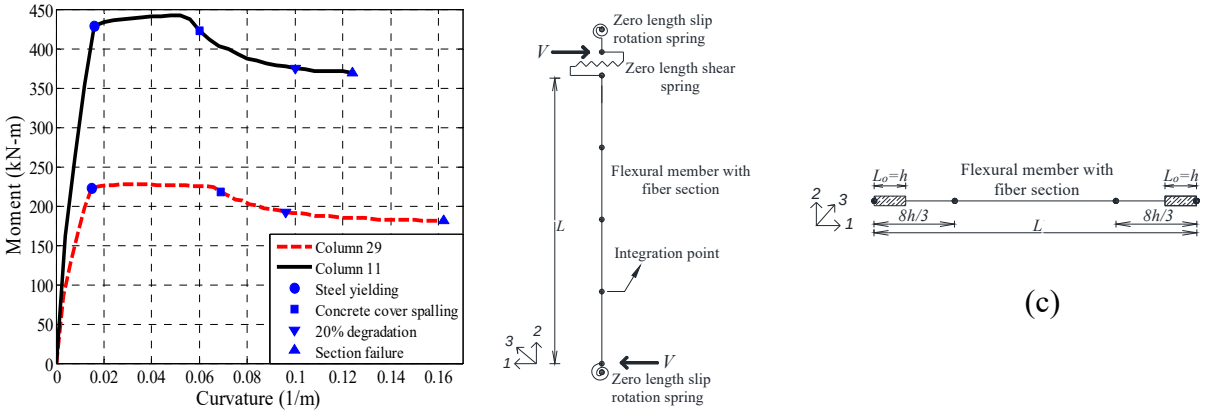

Figure 3 a) moment-curvature relationship for a single column (second column on the left in the second and fourth stories in Figure 2); spring model used for b) column with fixed ends, and c) beam with fixed ends.

3.1.2. Shear model

Recent earthquakes have shown that columns in older RC buildings with poor seismic detailing, including the hotel building considered in this paper, experience shear or flexure-shear failures. The shear model proposed by [37] can capture both the inelastic shear response and the shear failure. The lateral force-shear displacement envelope includes three distinct points corresponding to: (a) maximum shear strength and corresponding shear displacement; (b) onset of shear strength degradation and corresponding shear displacement; and (3) shear displacement at axial load failure.

Accordingly, the maximum shear strength, V_n, is predicted by the following expression [38]:

$$V_n = V_s + V_c = k\frac{A_v \cdot f_y \cdot d}{s} + k\left(\frac{0.5\sqrt{f_c'}}{a/d}\sqrt{1+\frac{P}{0.5\sqrt{f_c'}A_g}}\right)0.8\,\mathrm{A_g} \tag{14}$$

where A_v is the transverse reinforcement area within a spacing, s, in the loading direction; f_y is the transverse reinforcement yield strength (MPa); d is the section depth; f'_c is the compressive strength of concrete; a is the shear span of the element; P is the axial load; A_g is the gross area of the section; and k is a factor to account for ductility-related strength degradation. Shear displacements are calculated using a combination of two existing models, i.e., [37,39]. The shear displacement corresponding to peak strength, $\Delta_{v,n}$, is calculated as:

$$\Delta_{v,n} = \left(\frac{f_y\,\rho_l}{5000\cdot a/d\cdot\sqrt{P/A_g f_c'}} - 0.0004\right)\cdot L \tag{15}$$

where ρ_l is the longitudinal steel ratio and L is the length of the column. As described in [39], the shear displacement at the onset of shear failure can be adopted from [40]. Shear displacement at axial failure, denoted as θ_{axial} in Section 2.1, is obtained using the procedure given in [37], which requires the calculation of total lateral drift Δ_a/L. The latter is calculated using the equation proposed by [41]:

$$\frac{\Delta_a}{L} = \frac{4}{100} \cdot \frac{1+\tan^2\theta}{\tan\theta + P \cdot (\frac{s}{A_v \cdot f_y \cdot d_c \cdot \tan\theta})} \tag{16}$$

3.1.3. Bar slip model

When a reinforcing bar embedded in concrete is subjected to a tensile force, strain accumulates over the embedded length of the bar. This tensile strain causes the reinforcing bar to slip relative to the concrete in which it is embedded. Slip of longitudinal column bars at column ends (i.e., from the footing or beam-column joint) will cause rigid body rotation of the column. This rotation is not accounted for in flexural analysis, where the column ends are assumed to be fixed. The bar slip model used in this study was presented in [37]. This model assumes a stepped function for bond stress between the concrete and reinforcing steel over the embedment length of the bar. The bond stress is taken as $1 \cdot \sqrt{f'_c}$ MPa for elastic steel strains and as $0.5 \cdot \sqrt{f'_c}$ MPa for inelastic steel strains. The rotation due to slip, θ_s, is calculated as *slip/(d-c)*, where *slip* is the extension of the outermost tension bar from the column end, and *d* and *c* are the distances from the extreme compression fiber to the centroid of the tension steel and the neutral axis, respectively. Steel strains and neutral axis location, determined at each step during the moment curvature analysis, are used here to determine slip rotation under increasing moment or column lateral force. The column lateral displacement due to bar slip, Δ_{slip}, is equal to the product of the slip rotation and the column length ($\Delta_{slip}=\theta_s \cdot L$).

3.1.4. Total lateral response

The total lateral response of a RC column can be modeled using a set of springs in series in OpenSees. The flexure, shear and bar slip deformation models discussed in previous sections are each modeled by a spring or flexural line element. Each spring or element is subjected to the same lateral force. Initially, the total displacement response is the sum of the responses of each spring. A typical column element includes two zero-length rotational bar-slip springs at its ends, one zero-length shear spring, and a flexural element with five integration points (see Figure 3(b)). The shear behavior is modeled as uniaxial hysteretic material in direction 1 in Figure 3(b). The bar slip is modeled with two rotational springs at the column ends using uniaxial hysteretic material in direction 3. Finally, same vertical displacement is maintained between nodes of zero length elements in the vertical direction (i.e., direction 2), using the equalDOF restraint in OpenSees.

The three deformation components are simply added together to obtain the total response up to the peak strength of the column [37]. Rules are established for the post-peak behavior of the springs based on a comparison of the shear strength V_n, the yield strength V_y, and the flexural strength V_p required to reach the plastic moment capacity. By comparing V_n, V_y, and V_p, the columns can be classified into five different categories [37]: Category I: $V_n<V_y$, the shear strength is less than the lateral load causing yielding in the tension steel. The column fails in shear while the flexural behavior remains elastic; Category II: $V_y<V_n<0.95V_p$, the shear strength is greater than the yield strength, but less than the flexural strength of the column. The column fails in shear, but inelastic flexural deformation occurring prior to shear failure affects the post-peak behavior; Category III: $0.95V_p<V_n<1.05V_p$, the shear and flexural strengths are very close; Category IV: $1.05V_p<V_n<1.4V_p$: the shear strength is greater than the flexural strength of the column. It is to note that for both categories III and IV, the column experiences large overall deformations potentially leading to two different possible failure modes: (a) flexural failure (which can be reached when the maximum inter-storey drift exceeds 10%, see Section 2.1 for the definition of the onset of collapse limit state), and (b) shear

failure: inelastic shear deformations affect the post-peak behavior, and shear failure may occur as increasing displacements reach θ_{axial}; Category V: V_n<1.4V_n, the shear strength is much greater than the flexural strength of the column. The column fails in flexure while the shear behavior remains in the elastic range.

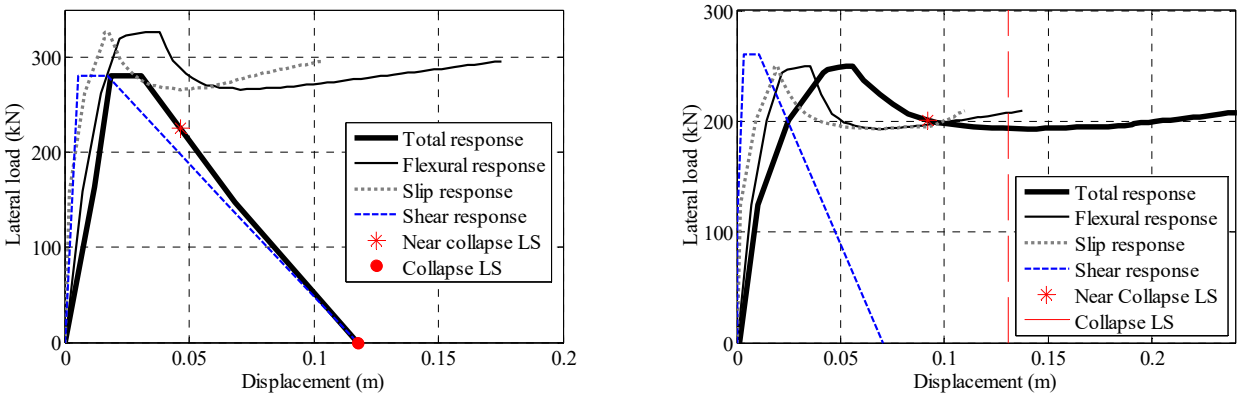

Figure 4: Different deformation components and the total lateral displacement for column 11 and 21 of the longitudinal frame, belonging to Category I (left) and Category IV (right)

Figure 4 shows the three different deformation components and the total lateral displacement for columns 11 and 21 of the analyzed frame, belonging to two different categories described above, i.e., Category I and Category IV, respectively (see Figure 2a). Failure modes are identified for all the columns of the case-study frames and reported on the right-hand side of the columns in Figure 2a. A comprehensive discussion on different issues about modeling part of the case-study frames is performed in [42].

3.2 The uncertainties characterization

Various sources of uncertainty are considered herein. In particular, the record-to-record variability (uncertainties in the representation of the ground motion), the uncertainties in component capacity models; in the mechanical material properties and in the construction details (the latter is also referred to as structural "defects"). For mechanical material properties and the construction details, the prior probability distributions are updated based on the available data for the case study, employing a Bayesian framework (see [12] for detailed description of the updating procedure).

3.2.1 Uncertainty in the representation of ground motions

The record selection for Cloud Analysis is particularly important. Here are few points to consider when selecting records for Cloud Analysis [9]: a) the records should be selected in a way that they cover a vast range of spectral acceleration values. In other words, the larger is the dispersion in S_a values, the smaller is the standard error of regression $\beta_{DCRLS|Sa}$; b) the records should be selected in such a way that a significant proportion (say more than 30%) of records have DCR_{LS} greater than unity; c) It is recommended to avoid selecting both horizontal components of the same recording unless the structural model is three-dimensional. Moreover, it is recommended to avoid selecting too many records from the same seismic event.

Two sets of 34 and 70 strong ground-motion records are selected from the NGA-West2 database (see [9] for the list of the records). The suite of 70 records covers a wide range of magnitudes between 5.5 and 7.9, and closest distance-to-ruptured area (denoted as R_{RUP}) up to around 40 km, as illustrated by the scatter diagram in Figure 5(a). The associated spectral shapes are shown in Figure 5(b). The soil average shear wave velocity in upper 30 m of soil,

V_{s30}, at the Holiday Inn hotel's site is around 218 m/sec. Accordingly, all selected records are chosen from NEHRP site classes C-D. The lowest useable frequency is set at 0.25 Hz, ensuring that the low-frequency content is not removed by the ground motion filtering process. There is no specific consideration on the type of faulting; nevertheless, all selected records are from strike-slip or reverse faults (consistent with California faulting). The records are selected to be free field or on the ground level. The set of 34 ground-motion records is extracted from the set of the 70 records. The only criterion for this selection is to limit the number of records from a single seismic event to be one (to avoid intra-event correlations).

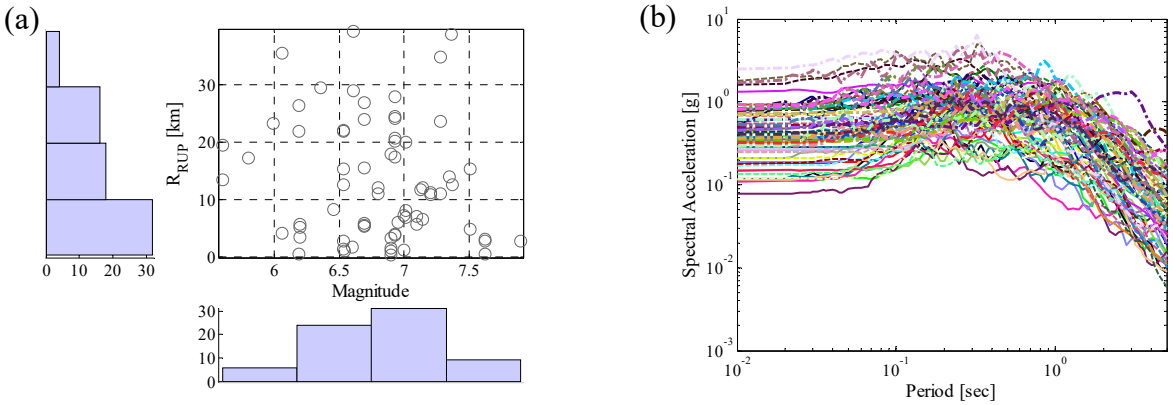

Figure 5 (a) Scatter diagram, and (b) Spectral shape, for the suite of the 70 ground-motion records.

3.3.2 Uncertainty in the component capacity models

Component capacities are modelled herein as the product of predictive formulas expressed as η_{Ci} and unit-median Log Normal variables ε_{Ci} accounting for the uncertainty in component capacity [8,11], according to the general format:

$$C_i = \eta_{Ci} \cdot \varepsilon_{Ci} \tag{17}$$

The expression for median capacities corresponding to the considered mechanism are described below. The median of the lognormal distribution of the maximum shear strength, V_n, is calculated according to Eq. 14 ($\eta_{Ci}=V_n$), while the relative COV has been provided in [38]. The median of the lognormal distribution of shear displacement corresponding to peak strength, $\Delta_{v,n}$, is calculated according to Eq. 15 ($\eta_{Ci}=\Delta_{v,n}$), while the relative COV has been assumed equal to 0.15 due the lack of specific data.

The median of the lognormal distribution of total lateral displacement, Δ_a, is calculated according to Eq. 16 ($\eta_{Ci}=\Delta_a$), while the relative COV has been taken as presented in [43].

Table 1 summarizes the component capacity variables, that have been considered herein, and the relative distributions.

Log-normal variable	COV	References
V_n	0.15	[38]
$\Delta_{v,n}$	0.15	[40]
Δ_a	0.26	[41,43]

Table 1 Logarithmic standard deviation values for component capacity models.

3.3.3 Uncertainty in the mechanical material properties and in the construction details

The probability distributions for the material mechanical properties and for the construction details (structural defects) are obtained using a Bayesian framework, updating the prior probability distributions with the available data for the specific case study [18]. The parameters identifying the prior probability distributions for the material mechanical properties

(compressive concrete strength for beams and columns at different floors, steel yielding force for beams and columns, compressive concrete ultimate strain, steel hardening slope) have been based on the values provided in Table 2. The probability distributions for the material mechanical properties are later updated employing the Bayesian framework for inference (see [12] for details of the updating procedure).

As said, Table 2 shows the statistics of the lognormal prior and posterior probability distributions for the material mechanical properties and the related references. Figure 6a illustrates the prior and posterior probability distributions of the concrete strength *fc1* (see Table 2).

Material	Prior distribution			Posterior distribution			References	Available data
	Type	Median	COV	Type	Median	COV		
f_{y1} (MPa)	LN	496	0.12	LN	488	0.07	[34,35]	[34,35]
f_{y2} (MPa)	LN	344	0.12	LN	339	0.07	[34,35]	[34,35]
f_{c1} (MPa)	LN	34.5	0.15	LN	39.1	0.11	[34]	[34,35]
f_{c2} (MPa)	LN	27.6	0.15	LN	31.5	0.11	[34]	[34,35]
f_{c3} (MPa)	LN	20.7	0.15	LN	23.5	0.11	[34]	[34,35]
e_{cu}	LN	0.006	0.40	LN	0.007	0.30	[44,45]	[34,35]
$\alpha_{hardening}$	LN	0.010	0.40	LN	0.011	0.31	[34]	[34]

Table 2 The uncertainty characterization for the material mechanical properties.

With regard to the construction detailing parameters, it has been assumed herein that 50% of the inspections verify the design values indicated in the original documents. Table 3 shows the prior and posterior probability distribution statistics for the spacing between the shear reinforcement for the columns, which is the only construction detailing variable assumed as uncertain herein. Figure 6b illustrates the prior and posterior probability distributions for the spacing between the shear reinforcement together with updated distribution based on the hypothesis that 50% of the inspections verify the design value (s=30.5cm). The updating procedure is described in detail in [12].

Defect	Prior distribution	Values	Reference	Posterior distribution	Median	COV
Shear rebars spacing	Uniform	30-40cm	[34]	Lognormal	35.5cm	0.18

Table 3 The uncertainty in spacing of shear rebars

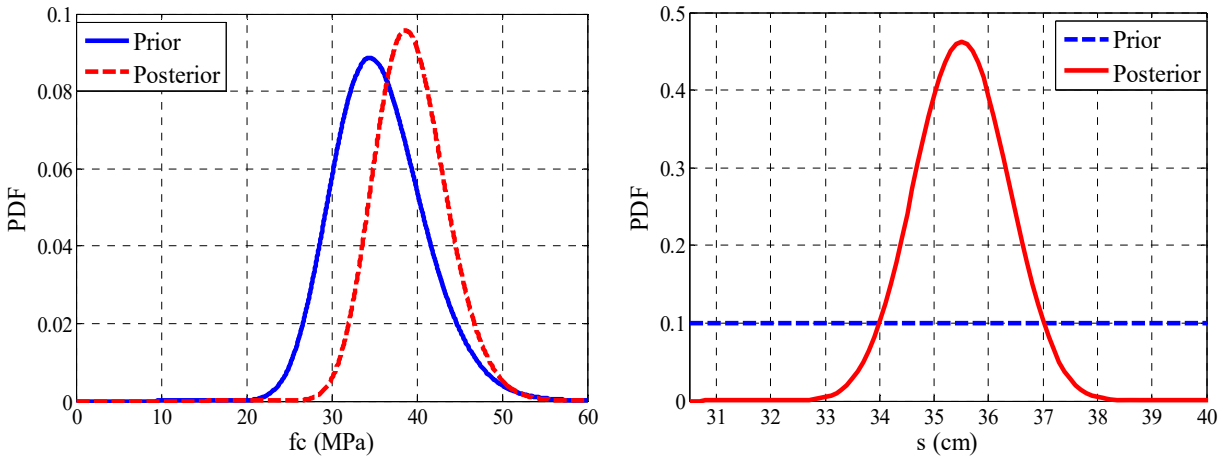

Figure 6 a) The prior and updated probability distributions for the concrete strength *fc1* (see Table 2); b) The uniform prior and updated probability distributions for the spacing of the shear rebars (see Table 3).

3.3 Cloud Analysis

Figures 7a show the scatter plots for Cloud data **D**={($S_{a,i}$, $DCR_{LS,i}$), i=1:34} for the case-study frame and for the set of the different realizations (each one is a simulated structural model through the standard Monte Carlo procedure plus a registered record). The grey-colored circles represent the *NoC* data, while the grey-colored with red edge squares indicate the *C* data or "collapse-cases" (see Section 2.4). In order to have a better representation of *NoC* data, an upper-bound limit of 5 is assigned to the horizontal DCR_{LS}-axis. It can be noted that, consistent with the Section 2.3 recommendations, the Cloud data not only covers a vast range of spectral acceleration values, but it also provides numerous data points in the range of DCR_{LS}>1. Figure 7a illustrates also Cloud Analysis regression prediction model (i.e., regression line and the estimated parameters, see Eq. 2) fitted to the *NoC* data. The Lognormal distribution displayed in Figure 7a denotes the distribution of DCR_{LS} given $S_a(T_1)$. Moreover, the line DCR_{LS}=1 corresponding to the onset of limit state (herein, Near-Collapse) is shown with red-dashed line. Finally, Figure 7a shows the 16th, 50th and 84th percentiles of the performance variable as a function of spectral acceleration, with and without considering the collapse cases. Figure 7b shows the same information for the larger set of 70 records/structural model realizations.

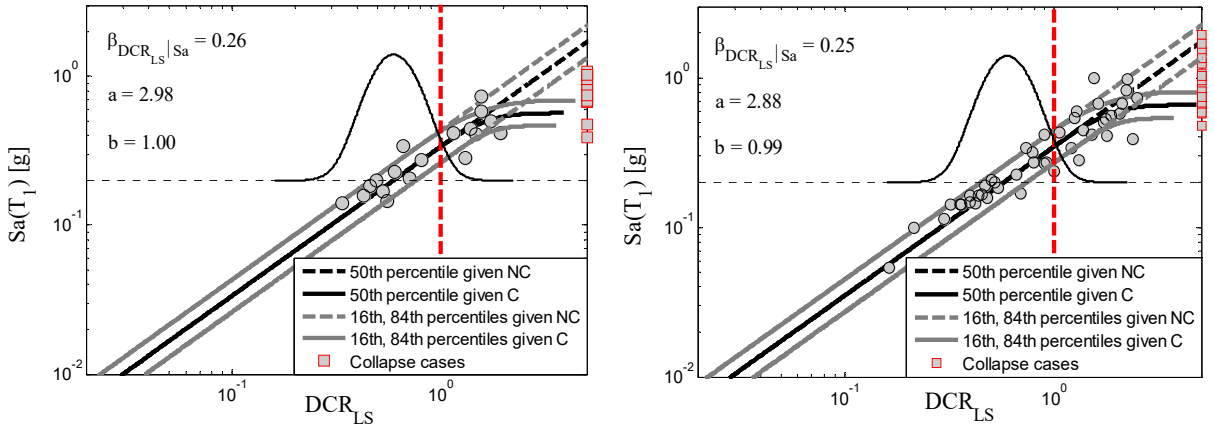

Figure 7 a) Cloud data and regression for the set of 34 records/realizations; b) Cloud data and regression for the set of 70 records/realizations

It is worth noting that the structural model realizations can also be generated through a Latin Hypercube (LHS described briefly in the next section, [46-48]) sampling scheme. This is done herein but the corresponding Cloud Analysis results are not reported for brevity. However, the fragility and risk results are reported later.

3.4 IDA with Latin Hypercube Sampling (LHS)

The LHS belongs to the category of advanced stratified sampling techniques which result in a good estimate of statistical moments of response using small-sample simulation. The basic feature of LHS is that the range of univariate random variables is divided into N intervals (N is a number of simulations); the values from the intervals are then used in the simulation process (random selection, median or the mean value). The selection of the intervals is performed in such a way that the range of the probability distribution function of each random variable is divided into intervals of equal probability, 1=N. The samples are chosen directly from the distribution function based on an inverse transformation of the univariate distribution function. The representative parameters of variables are selected randomly, being based on random permutations of integers k=1,2,..,N. Every interval of each variable must be used only

once during the simulation. The generation of the LHS is then completed by randomly pairing (without replacement) the resulting values for each of the random variables. Unfortunately, the nature of LHS does not allow us to determine a priori the appropriate sample size N to achieve a certain confidence level. Still, the use of a relatively high N that is substantially larger than the number of parameters will always result to reasonably accurate estimates for practical purposes. The optimal N to use is obviously a function of the number of random variables and their influence on the response is a subject of further research [23].
The LHS has been paired up with incremental dynamic analysis (IDA) in order to consider both the record-to-record variability and the epistemic uncertainties (eg, [22-24]). In this work, for the sake of comparison with the literature, Monte Carlo with LHS has been performed for N=34 and for N=80 realizations of the frame, a relatively high number that has been chosen to allow pinpoint accuracy in our estimates (the number of uncertain variable is 11). Thus, by performing IDA on each of the N realizations, 34×34=1156 and 80×34=2720 IDA curves have been obtained, respectively. Each IDA curve traces the variation in DCR_{LS} for a given realization of the structural model as a function of $Sa(T_1)$ as the record's amplitude is linearly scaled up. As explained in Sect. 3.4, the spectral acceleration values at DCR_{LS}=1, denoted as $Sa^{DCR=1}$, are used in order to obtain the IDA-based fragilities [11].

3.5 Mean Value First-order second-moment (MVFOSM) method

The MVFOSM method, which is based on the calculation of the first two moments of a nonlinear function, is an approximate method for propagating the uncertainties (e.g. [23,49]). The number of simulations required is only $2K+1$, where K is the number of uncertain variables considered in the study. Let the log of the Sa capacity denoted as $\ln Sa^{DCR=1}$ be a function f of the uncertainties vector:

$$\ln S_a^{DCR=1} = f(\theta) = \mathrm{f}(\theta_1, \theta_2, ..., \theta_k) \tag{22}$$

where f is a function of the random variables for the given limit state and θ is the vector of the random uncertain modeling parameters. It should be noted that the Sa capacity is calculated from the median of IDA curves.

In the first place, the base-case value of f denoted as $\ln Sa^{DCR=1,0}$, that corresponds to all random variables being set equal to their mean $m_{\theta k}$ is calculated. The remaining $2K$ simulations are obtained by shifting each parameter θ_k from its mean by $\pm 1.7\sigma_{\theta k}$ [25], while all other variables remain equal to their mean $m_{\theta k}$. When the θ_k parameter is perturbed, the logs of the median Sa-capacities are denoted as $\ln Sa^{k+}$ and $\ln Sa^{k-}$, where the sign indicates the direction of the shift. Since the number of simulations required is $2K+1$ and K=11 in this study, 23×34=782 (where 34 is the number of records) IDA curves have been obtained, based on the previous recommendations.

According to MVFOSM, the nonlinear function f can be approximated using a Taylor expansion to obtain its first and second moments. Following the notation of Eq. 22, the function f= $\ln Sa^{DCR=1}$ is expanded around the mean value denoted as $\bar{\theta}$ [50]:

$$f(\theta) \approx f(\bar{\theta}) + \sum_{k=1}^{K} (\theta_k - \mathrm{m}_{\theta_k}) \frac{df}{d\theta_k}\bigg|_{\bar{\theta}} + \frac{1}{2}\sum_{k=1}^{K} (\theta_k - \mathrm{m}_{\theta_k})^2 \frac{d^2 f}{d\theta^2_k}\bigg|_{\bar{\theta}} \tag{23}$$

The gradient and curvature of f can be approximated with a finite difference approach, which is why 2K+1 simulations were needed. The random parameters are set equal to their mean to obtain $\ln Sa^{DCR=1,0}$ and then each random parameter is perturbed as described above. Thus, the first and the second derivative of f with respect to θ_k, will be:

$$\frac{df}{d\theta_k} \approx \frac{\ln S_a^{k+} - \ln S_a^{k-}}{2 \cdot 1.7 \cdot \sigma_{\theta_k}}$$
$$\frac{d^2 f}{d\theta^2_k} \approx \frac{\ln S_a^{k+} - 2 \cdot \ln S_a^{DCR=1}{}_{,0} + \ln S_a^{k-}}{1.7 \cdot \sigma^2_{\theta_k}} \quad (24)$$

Truncating after the linear terms in Eq. 23 provides a first-order approximation for the limit-state mean-log capacities, where they are going to be equal to the base-case values ln $S_a^{DCR=1}{}_{,0}$ (the linear term is going to be equal to zero). A more refined estimate is the mean-centered, second-order approximation, which according to Eq.23 can be estimated as [23]:

$$m_{\ln Sa^{DCR=1}} \approx \ln S_a^{DCR=1}{}_{,0} + \sum_{k=1}^{K} \frac{1}{2} \frac{d^2 f}{d\theta^2_k} |_{\bar{\theta}} \cdot \sigma_{\theta^2_k} \quad (25)$$

Thus the median S_a capacity, assuming lognormality, comes out to be:

$$\hat{S}_a^{DCR=1} = \exp(m_{\ln Sa^{DCR=1}}) \quad (26)$$

while, using a first-order approximation, the standard deviation of the logs is estimated as:

$$\beta_{\ln Sa^{DCR=1}} \approx \sum_{k=1}^{K} (\frac{df}{d\theta_k} |_{\bar{\theta}})^2 \sigma_{\theta^2_k} \quad (27)$$

It should be noted that the above statistics refer to the *Sa* capacity as calculated from the median IDA curve and total dispersion will need to combine also the effect of record-to-record variability. In this work, the SRSS approach has been used in order to combine the dispersion due to the structural modeling uncertainties and the record-to-record variability.

3.6 Fragility curves comparison

Figure 8a illustrates the Cloud-based Robust Fragility curve (black solid line) and its plus/minus two standard deviation confidence bands (grey dashed lines). The Robust Fragility curve and its confidence interval is obtained following the procedure described in Section 2.5 (see [9] for more details). As mentioned in Section 2.5, one distinct advantage gained by calculating the Robust Fragility lies in the estimation of its confidence band. In Figure 8a the Cloud-based Robust Fragility curve is compared with the fragility curve obtained through Cloud Analysis (black dashed line) with the consideration only of the record to record (R2R) variability. Moreover, also the the site-specific hazard (at T=1 sec, from USGS National Seismic Hazard Mapping Project website (http://earthquake.usgs.gov/hazards, red solid line) is shown in Figure 8a. As it can be seen from Figure 8a, Cloud-based Robust Fragility curve with the consideration of all the sources of uncertainty present a reduction both in median capacity and in the dispersion with respect to the fragility curve obtained through Cloud Analysis with the consideration only of the record-to-record variability.

Figure 8b illustrates the Cloud-based Robust Fragility curve (black solid line) with its plus/minus one standard deviation confidence bands (grey dashed lines) and the fragility curves (thin grey solid lines) obtained based on Cloud Analysis through the generation of different sets of realizations (10 different sets) of the structural model. It can be observed that the different simulations of the cloud-based fragility curves are contained within the plus/minus one standard deviation interval of the robust fragility curve. The fragility curve based on the Cloud Analysis of 70 records/structural model realizations is also shown in Figure 8b in solid blue lines. The figure also illustrates how the cloud-based fragility curves would shift if the LHS procedure is used for stratified sampling of the structural model parameters instead of the standard Monte Carlo procedure proposed herein (for both sets of 34 and 70 records plotted as black dotted and blue dotted lines, respectively). It can be observed that the differences

between the number of records/extractions and the type of simulation (random versus stratified) is again contained within one standard deviations away from the Robust Fragility curve (obtained based 34 record/realizations and standard Monte Carlo sampling of the structural model parameters). This underlines the utility of the confidence bands, that represent a reliable interval, in which the "true" fragility curve would lie with a prescribed probability/confidence level. Moreover, it can be observed that the fragility curve based on 70 records/LHS-generated realizations marks an increase in the dispersion with respect to the rest of the curves.

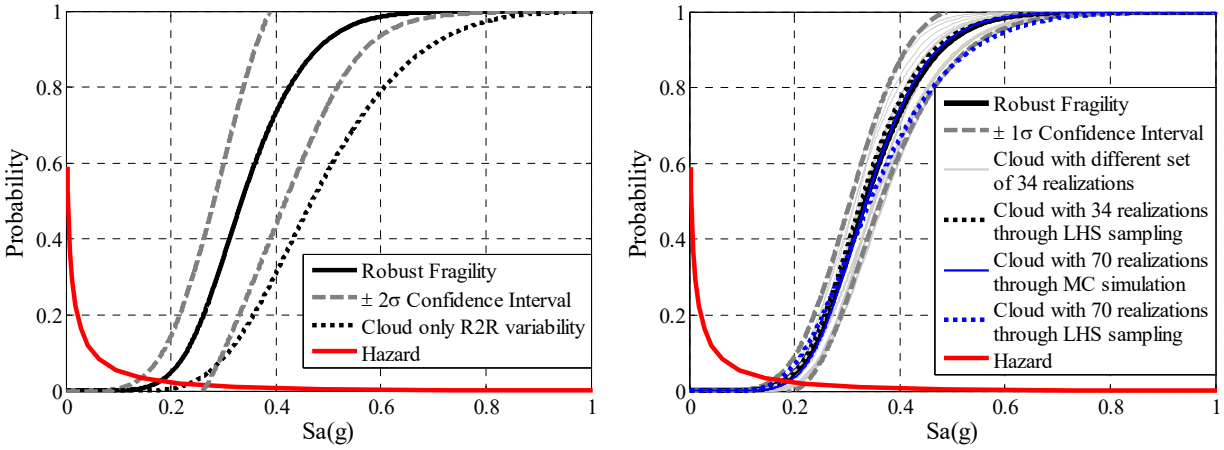

Figure 8 a) Robust Fragility and its plus/minus two standard deviation confidence interval and Cloud-based fragility curve, considering only the R2R variability; b) Robust Fragility and its plus/minus one standard deviation confidence interval, Cloud-based fragility curves based on 10 different 34 records/MC-based realizations, Cloud-based fragility curves based on 70 records/MC-based realizations, 34 records/LHS-based realizations and 70 records/LHS-based realizations of the uncertainties vector θ

Figure 9 illustrates the comparison between the (cloud-based) Robust Fragility curve and its plus/minus two standard deviations interval, the IDA-based fragility curves obtained using the LHS, with 34 and 80 realizations of the structural model (plotted in blue solid and blue dashed lines, respectively), and the fragility curve obtained through MVFOSM approach (in black dashed line). As it can be seen from Figure 9, the different fragility curves are close in terms of median capacity. The difference between the IDA-based/LHS fragilities and the IDA-based/MVFOSM fragility curves is contained within the plus/minus two standard deviations interval of the Robust Fragility. It can be observed that the Cloud-based Robust Fragility is quite close to the fragility curves obtained through the IDA-based/LHS and IDA-based/MVFOSM approaches, while the computational effort is sensibly lower. As shown in Table 1, the Cloud-based Robust Fragility requires number of analyses equal to the number of the records in the chosen set (34 and 70 for the case study). To implement IDA using LHS and MVFOSM, the necessary analyses are in the order of thousands and hundreds, respectively. In particular, for IDA paired up with LHS the number of required analysis is the product of the number of structural realizations, the number of the selected records and the number of steps for IDA procedure. For implementing the IDA paired up with the MVFOSM approach, the number of required analysis is the product of two times the number of the uncertain variables plus one (the base-case value of f that corresponds to all random variables being set equal to their mean), the number of the selected records and the number of steps for IDA procedure.

It is important to note that these results refer to the specific case study and additional comparisons are needed to validate these results. Based on the site-specific hazard shown in Figure 9, it can be noted that the difference between the Cloud-based Robust Fragility curve and IDA-based/LHS and IDA-based/MVFOSM fragility curves are more accentuated in the zone

of very small hazard values. This observation is further validated by risk calculations reported in Table 4.

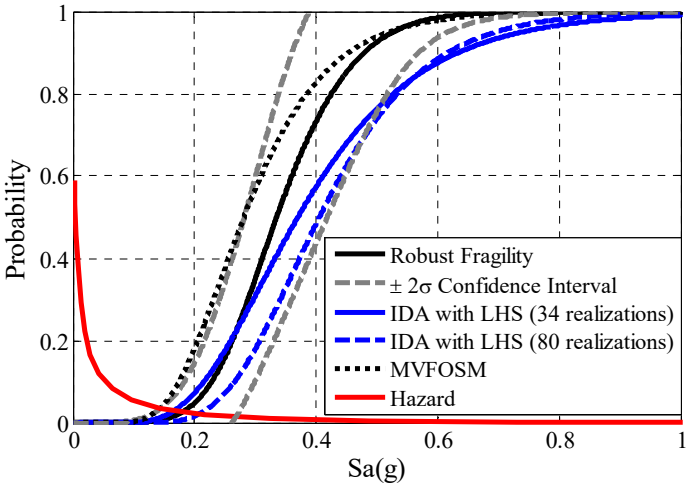

Figure 9 Comparison between Cloud-based Robust Fragility curve and its plus/minus two standard deviations intervals, IDA-based fragility curves obtained using LHS sampling with 34 and 80 realizations and IDA-based fragility curve obtained through MVFOSM approach.

Table 4 summarizes for all the procedures discussed herein, the number of analyses required and the mean annual frequencies of exceeding the Near-Collapse limit state (i.e., risk obtained by integrating the fragility and site-specific hazard curve) denoted by λ_{LS} corresponding to the different fragility curves. In particular, R_F denotes the risk corresponding to the Robust fragility curve and $R_{F\pm2\sigma\chi}$ define the risk values associated with Robust Fragility plus/minus its two standard deviation confidence intervals. It can be noted that Cloud-based Robust fragility curves (with 34 or 70 realizations through standard MC simulation or LHS sampling) with their plus/minus two standard deviation confidence bands provide reliable results in term of risk with respect to IDA-based LHS and MVFOSM approach fragility curves.

Type of procedure	*Number of analyses*	λ_{LS} using the Robust fragility		
		$R_{F+2\sigma\chi}$	R_F	$R_{F-2\sigma\chi}$
RF with 34 realizations through MC sim	34	7.4×10^{-3}	1.1×10^{-2}	1.5×10^{-2}
RF with 34 realizations through LHS	34	7.8×10^{-3}	1.0×10^{-2}	1.4×10^{-2}
RF with 70 realizations through MC sim	70	7.9×10^{-3}	1.0×10^{-2}	1.2×10^{-2}
RF with 70 realizations through LHS	70	7.7×10^{-3}	1.0×10^{-2}	1.4×10^{-2}
MVFOSM approach	7820	-	1.5×10^{-2}	-
IDA with LHS (34 realizations)	11560	-	1.0×10^{-2}	-
IDA with LHS (80 realizations)	27200	-	9.0×10^{-3}	-

Table 4 Number of analyses required and the mean annual frequency of exceeding the limit state for the alternative procedures.

4 CONCLUSIONS

In this work, a modified version of Cloud Analysis considering the (eventual) cases of global dynamic instability, based on coupling the simple regression in the logarithmic space of structural response versus seismic intensity for a suite of registered records with logistic regression, has been implemented to propagate both record-to-record variability and modelling uncertainties. For each of the registered records within the suite of ground motion records, a different realization of the structural model has been generated through a standard Monte Carlo Simulation procedure. A Bayesian version of the Cloud method is employed, in which the uncertainty in the structural fragility model parameters is considered. This leads to a ro-

bust fragility estimate and a desired confidence interval defined around it. The longitudinal frame of an existing building in Van Nuys, CA, modeled with the consideration of the flexural-shear-axial interaction, has been employed to demonstrate this procedure. The selection of the suite of ground motion records for the case study has been based on a set of criteria that ensure the statistical significance of the linear regression in predicting the structural response as a function of the intensity measure.

It is observed that, for the case study frame, Cloud-based Robust Fragility curve with the consideration of both record-to-record variability and structural modelling uncertainties leads to a reduction both in median and in the dispersion of the fragility curve with respect to the Cloud-based fragility considering only R2R variability. Moreover, the Cloud-based Robust Fragility curve is very close to the results provided by IDA-based LHS and MVFOSM fragility curves, while the computational effort is sensibly lower. These observations refer to the specific case study and additional comparisons needed to validate these results. Based on the site-specific hazard, it can be noted that the difference between the Cloud-based Robust Fragility curve and the IDA based fragility curves obtained using the LHS and the MVFOSM approach are more accentuated in the zone of very small hazard values. Thus, it can be noted that Cloud-based Robust Fragility curves (with 34 or 70 realizations through standard MC simulation or LHS sampling) with their plus/minus two standard deviation confidence bands provide reliable results in term of risk with respect to IDA-based LHS and MVFOSM fragility curves. Consequently, and with specific reference to the case-study frame, the Cloud-based Robust Fragility procedures provides --in an extremely efficient manner-- reliable risk estimates.

ACKNOWLEDGEMENTS

This work is supported in part by the executive Project ReLUIS-DPC 2014/2018. This support is gratefully acknowledged. The first author's Ph.D. grant is funded by a scholarship defined within the University of Naples's Ph.D. program of Structural, Geotechnical and Seismic Engineering. This support is gratefully acknowledged. The case-study frame is modeled during the first author's research exchange period at Ohio State University and under the supervision of Prof. Halil Sezen. His support is gratefully acknowledged. Last but not least, the authors would also like to thank Dr. Hossein Ebrahimian for providing the authors with the routine for MCMC-based Robust Fragility calculation. This support is gratefully acknowledged.

REFERENCES

[1] C.A. Cornell, H. Krawinkler, Progress and challenges in seismic performance assessment. *PEER Center News*, 3 (2): 1-2, 2000.

[2] D. Vamvatsikos, C.A. Cornell, Incremental dynamic analysis. *Earthquake Engineering and Structural Dynamics*, 31(3), 491-514, 2002.

[3] P. Bazzurro, C.A. Cornell, N. Shome, J.E. Carballo, Three proposals for characterizing MDOF nonlinear seismic response. *Journal of Structural Engineering (ASCE)*, 124 (11): 1281-1289, 1998.

[4] F. Jalayer, C.A. Cornell, Alternative non-linear demand estimation methods for probability-based seismic assessments. *Earthquake Engineering and Structural Dynamics*, 38(8): 951-972, 2009.

[5] J.W. Baker, Probabilistic structural response assessment using vector-valued intensity measures. *Earthquake Engineering and Structural Dynamics*, 36(13), 1861-1883, 2007.

[6] N. Shome, C.A. Cornell, P. Bazzurro, J.E. Carballo, Earthquakes, records, and nonlinear responses. *Earthquake Spectra*, 14(3), 469-500, 1998.

[7] F. Jalayer, Direct Probabilistic seismic analysis: implementing non-linear dynamic assessments. *Ph.D. dissertation*, Stanford University, California, 2003.

[8] F. Jalayer, R. De Risi, G. Manfredi, Bayesian Cloud Analysis: efficient structural fragility assessment using linear regression. *Bulletin of Earthquake Engineering*, 13(4), 1183-1203, 2005.

[9] F. Jalayer, H. Ebrahimian, A. Miano, G. Manfredi, H. Sezen, Analytical fragility assessment using un-scaled ground motion records. *Earthquake Engineering and Structural Dynamics*, 2017; (Submitted).

[10] C.A. Cornell, F. Jalayer, R.O. Hamburger, D.A. Foutch, Probabilistic basis for 2000 SAC federal emergency management agency steel moment frame guidelines. *Journal of Structural Engineering*, 128(4), 526-533, 2002.

[11] F. Jalayer, P. Franchin, P. Pinto, A scalar damage measure for seismic reliability analysis of RC frames. *Earthquake Engineering and Structural Dynamics*, 36(13), 2059-2079, 2007.

[12] F. Jalayer, L. Elefante, I. Iervolino, G. Manfredi, Knowledge-based performance assessment of existing RC buildings. *Journal of Earthquake Engineering*; 15 (3): 362-389, 2011.

[13] J.W. Hickman, PRA procedures guide: a guide to the performance of probabilistic risk assessments for nuclear power plants. *NUREG/CR-2300*, U.S. Nuclear Regulatory Commission, Washington, DC, 1983.

[14] R.P. Kennedy, M.K. Ravindra, Seismic fragilities for nuclear power plant risk studies. *Nuclear Engineering and Design*, 79(1), 47-68, 1984.

[15] J.W. Reed, R.P. Kennedy, Methodology for developing seismic fragilities. *Final Report TR-103959*, EPRI, 1994.

[16] B.R. Ellingwood, O.C. Celik, K. Kinali, Fragility assessment of building structural systems in Mid‐America. *Earthquake Engineering and Structural Dynamics*, 36 (13): 1935-1952, 2007.

[17] O.C. Celik, B.R. Ellingwood, Seismic fragilities for non-ductile reinforced concrete frames–Role of aleatoric and epistemic uncertainties. *Structural Safety*, 32(1): 1-12, 2010.

[18] F. Jalayer, I. Iervolino, G. Manfredi, Structural modeling uncertainties and their influence on seismic assessment of existing RC structures. *Structural Safety*, 32 (3): 220-228, 2010.

[19] P. Franchin, P.E. Pinto, P. Rajeev, Confidence factor?. *Journal of Earthquake Engineering*, 14(7), 989-1007, 2010.

[20] R.E. Melchers, Structural reliability. *Horwood*, 1987.

[21] M.I.J. Schotanus, P. Franchin, A. Lupoi, P.E. Pinto, Seismic fragility analysis of 3D structures. *Structural Safety*, 26(4), 421-441, 2004.

[22] M. Dolsek, Incremental dynamic analysis with consideration of modeling uncertainties. *Earthquake Engineering and Structural Dynamics*, 38(6), 805-825, 2009.

[23] D. Vamvatsikos, M. Fragiadakis, Incremental dynamic analysis for estimating seismic performance sensitivity and uncertainty. *Earthquake Engineering and Structural Dynamics*, 39(2), 141-163, 2010.

[24] D. Celarec, M. Dolšek, The impact of modelling uncertainties on the seismic performance assessment of reinforced concrete frame buildings. *Engineering Structures*, 52, 340-354, 2013.

[25] A.B. Liel, C.B. Haselton, G.G. Deierlein, J.W. Baker, Incorporating modeling uncertainties in the assessment of seismic collapse risk of buildings. *Structural Safety*, 31(2), 197-211, 2009.

[26] H. Krawinkler, Challenges and progress in performance-based earthquake engineering. *International Seminar on Seismic Engineering for Tomorrow-In Honor of Professor Hiroshi Akiyama*, Tokyo, Japan, November 26, 1999.

[27] Ditlevsen O. and Madsen H.O. (1996). Structural reliability methods. Wiley: New York.

[28] *Eurocode 8* Design of structures for earthquake resistance, 2007.

[29] P.H. Galanis, J.P. Moehle, Development of Collapse Indicators for Risk Assessment of Older-Type Reinforced Concrete Buildings. *Earthquake Spectra*, 31(4), 1991-2006, 2015.

[30] N. Shome, C.A. Cornell, Probabilistic seismic demand analysis of nonlinear structures. *Report No. RMS35*, Stanford University, CA, 2002.

[31] F. Jalayer, H. Ebrahimian, Seismic risk assessment considering cumulative damage due to aftershocks. *Earthquake Engineering and Structural Dynamics*, 46(3), 369-389, 2016.

[32] J.L. Beck, S.K. Au, Bayesian updating of structural models and reliability using Markov Chain Monte Carlo simulation. *Journal of Engineering Mechanics (ASCE)*, 128 (4): 380-391, 2002.

[33] F. McKenna, OpenSees: a framework for earthquake engineering simulation. *Computing in Science and Engineering*, 13(4), 58-66, 2011.

[34] H. Krawinkler, Van Nuys hotel building testbed report: exercising seismic performance assessment. *Pacific Earthquake Engineering Research Center*, University of California, Berkeley, 2005.

[35] M.S. Islam, Analysis of the Northridge earthquake response of a damaged non-ductile concrete frame building. *The structural design of tall buildings*, 5(3), 151-182, 1996.

[36] M.H. Scott, G.L. Fenves, Plastic hinge integration methods for force-based beam–column elements. *Journal of Structural Engineering*, 132(2), 244-252, 2006.

[37] E.J. Setzler, H. Sezen, Model for the lateral behavior of reinforced concrete columns including shear deformations. *Earthquake Spectra*, 24(2), 493-511, 2008.

[38] H. Sezen, J.P. Moehle, Shear strength model for lightly reinforced concrete columns. *Journal of Structural Engineering*, 130(11), 1692-1703, 2004.

[39] H. Sezen, Shear deformation model for reinforced concrete columns. *Structural Engineering and Mechanics*, 28(1), 39-52, 2008.

[40] M. Gerin, P. Adebar, Accounting for shear in seismic analysis of concrete structures. *Proc., 13th World Conference on Earthquake Engineering*, 1-6, 2004.

[41] K.J. Elwood, J.P. Moehle, Axial capacity model for shear-damaged columns. *ACI Structural Journal*, 102, 578-587, 2005.

[42] A. Miano, H. Sezen, F. Jalayer, A. Prota, Performance based comparison of effectiveness of building retrofit methods. *Earthquake Spectra*, 2017 (Submitted).

[43] K.J. Elwood, J.P. Moehle, Shake table tests and analytical studies on the gravity load collapse of reinforced concrete frames (No.1). *Pacific Earthquake Engineering Research Center*, 2003.

[44] H.E. Roy, M.A. Sozen, A model to simulate the response of concrete to multi-axial loading. *University of Illinois Engineering Experiment Station*. University of Illinois, 1963.

[45] J.B. Mander, M.J. Priestley, R. Park, Theoretical stress-strain model for confined concrete. *Journal of structural engineering*, 114(8), 1804-1826, 1988.

[46] J.C. Helton, F.J. Davis, Latin hypercube sampling and the propagation of uncertainty in analyses of complex systems. *Reliability Engineering and System Safety*, 81(1), 23-69, 2003.

[47] M.D. McKay, W.J. Conover, R. Beckman, A comparison of three methods for selecting values of input variables in the analysis of output from a computer code. *Technometrics*, 21(2):239–245, 1979.

[48] D. Novák, M. Vořechovský, B. Teplý, FReET: Software for the statistical and reliability analysis of engineering problems and FReET-D: Degradation module. *Advances in Engineering Software*, 72, 179-192, 2014.

[49] J.W. Baker, C.A. Cornell, Uncertainty propagation in probabilistic seismic loss estimation. *Structural Safety*, 30(3), 236-252, 2008.

[50] C. Menum, CE 204: Notes of Structural Reliability. Stanford University, California, 2000.